

The importance of Icelandic ice sheet growth and retreat on mantle CO₂ flux

John J. Armitage¹, David J. Ferguson², Kenni D. Petersen³, and Timothy T. Creyts⁴

¹Dynamique des Fluides Géologiques, Institut de Physique du Globe de Paris, Paris, France

²School of Earth and Environment, University of Leeds, Leeds, U.K.

³Department of Geoscience, University of Aarhus, Aarhus, Denmark

⁴Lamont-Doherty Earth Observatory, Columbia University, U.S.A

Key Points:

- We combine a new history of Icelandic ice-cover with a forward model of magma generation.
- Peak mantle CO₂ flux is non-linearly related to magmatic eruption rates.
- Icelandic CO₂ degassing likely peaked first at 60 ka, and secondly with three pulses between 20 and 10 ka.

15 **Abstract**

16 Climate cycles may significantly affect the eruptive behavior of terrestrial volcanoes due
 17 to pressure changes caused by glacial loading, which raises the possibility that climate
 18 change may modulate CO₂ degassing via volcanism. In Iceland, magmatism is likely to
 19 have been influenced by glacial activity. To explore if deglaciation therefore impacted
 20 CO₂ flux we coupled a model of glacial loading over the last ~120 ka to melt generation
 21 and transport. We find that a nuanced relationship exists between magmatism and glacial
 22 activity. Enhanced CO₂ degassing happened prior to the main phase of late-Pleistocene
 23 deglaciation, and it is sensitive to the duration of the growth of the ice sheet entering
 24 into the LGM, as well as the rate of ice loss. Ice sheet growth depresses melting in the
 25 upper mantle, creating a delayed pulse of CO₂ out-gassing as the magmatic system re-
 26 covers from the effects of loading.

27 **1 Introduction**

28 Evidence from several tectonic settings indicates that glaciated volcanic systems
 29 respond to changing ice volumes (Glazner, Manley, Marron, & Rojstaczer, 1999; Jellinek,
 30 Mange, & Saar, 2004; Jull & McKenzie, 1996; MacLennan, Jull, McKenzie, Slater, & Grönvöld,
 31 2002; Rawson et al., 2016; Sigvaldsson, Annertz, & Nilsson, 1992), and suggests there was
 32 a widespread volcanic response to late-Pleistocene ice retreat (Huybers & Langmuir, 2009).
 33 The most compelling evidence for climate-coupled volcanism comes from Iceland, where
 34 changes in early Holocene lava volumes and magma chemistry are consistent with de-
 35 pressurization during glacial unloading (Jull & McKenzie, 1996; MacLennan et al., 2002;
 36 Sinton, Grönvöld, & Saemundsson, 2005). Magma generation here occurs due to pressure-
 37 release melting, as the mantle up-wells beneath rift zones. Although the net change in
 38 overburden pressures from variations in ice cover have been relatively small, the high rates
 39 of change associated with glacial activity can produce significant short-term fluctuations
 40 in magmatic output (Jull & McKenzie, 1996; Pagli & Sigmundsson, 2008; Schmidt et al.,
 41 2013), similar to those hypothesised to occur at ocean ridges due to sea-level variation
 42 (Burley & Katz, 2015; Crowley, Katz, Huybers, Langmuir, & Park, 2015; Huybers & Lang-
 43 muir, 2009; Lund & Asimow, 2011). Carbon readily partitions into magmas during par-
 44 tial melting (Rosenthal, Hauri, & Hirschmann, 2015) and is released as a CO₂ rich fluid/vapour
 45 as the magma ascends through the crust, making volcanism the primary pathway for trans-
 46 porting carbon from the Earth's mantle to the atmosphere (Dasgupta & Hirschmann,
 47 2010). However, carbon does not enter the melt uniformly during partial melting and
 48 is concentrated in early formed magma. Therefore the extent to which glacially driven
 49 changes in primary magma generation alter the flux of CO₂ depends on where in the melt-
 50 ing column melt production is enhanced (or suppressed), the rate of melt transport, and
 51 the history of ice sheet growth and retreat.

52 Global data sets of the number of volcanic eruptions throughout the Pleistocene
 53 would suggest there is a correlation between climatic change and volcanism (Huybers
 54 & Langmuir, 2009), yet data resolution makes testing this association difficult. It is thought
 55 that CO₂ and the trace element Nb have a relatively similar behaviour during decom-
 56 pression melting (Saal, Hauri, Langmuir, & Perfit, 2002), and as such Nb compositions
 57 can be used to gauge the quantity of CO₂ erupted. In Iceland there are just over 300 pub-
 58 lished dated analysis of the Nb composition of Pleistocene lavas (Eason, Sinton, Grönvöld,
 59 & Kurz, 2015; Gee, Taylor, Thirwall, & Murton, 1998). This is arguably the most com-
 60 plete geochemical record of Nb compositions within a region that experienced significant
 61 Pleistocene deglaciation. In this study we take a new approach, and use a high resolu-
 62 tion model of ice sheet history to drive a forward model of melt generation and trans-
 63 port, and predict CO₂ degassing. We validate the model predictions against the seismic
 64 structure imaged below Iceland, and the observed crustal thickness. We subsequently
 65 explore under what conditions climate and magmatism might be related, and the im-
 66 plications for CO₂ degassing.

67 **2 Methods**

68 **2.1 Modelling of Melt Generation and Transport**

69 To investigate the impact of glacial activity on melt productivity, melt composition,
 70 and CO₂ flux, we used a model of magma generation and transport coupled to a
 71 model of the flexure of a viscoelastic beam for the response to change in load due to the
 72 ice sheet history (see Supplementary Material). The coupled model consists of a flexural
 73 model of the surface displacement due to the changing surface load as the ice sheet
 74 changes in thickness. This model of surface displacement is then coupled to either a 1D
 75 vertical column or a 2D corner flow model where the flow of the mantle is prescribed at
 76 either an upwelling rate of 10 or 20 mm yr⁻¹, or lateral spreading rate of 10 mm yr⁻¹. We
 77 use these two upwelling rates to cover the uncertainty in the exact rate of vertical as-
 78 cent the mantle below Iceland due to mantle buoyancy. The upwelling column, which
 79 spans a depth range of 300 to 30 km, is perturbed by the displacement due to loading,
 80 where the viscoelastic decay time of the load is set to 1000 yrs. The upper surface of the
 81 melting model is held at 30 km to be consistent with the Moho depth, which is in the
 82 range of 20 to 40 km below Iceland (Jenkins et al., 2018). Carbon partitioning into the
 83 melt is assumed to be governed by the coefficients derived by (Rosenthal et al., 2015).
 84 We use a mantle source composition for Nb of 1.627 ppm, which is intermediate between
 85 the end-member sources for Icelandic melts identified by (Shorttle & MacLennan, 2011).
 86 To approximate the melting of the multiple source lithologies we chose a solidus-depletion
 87 gradient of 600 °C which is intermediate between that of melting experiments on depleted
 88 mantle, 900 °C (Wasylenski, Baker, Kent, & Stopler, 2003) and fertile mantle 300 °C (Scott,
 89 1992).

90 The surface expression of partial melting to glacial loading/unloading is influenced
 91 primarily by the rate at which the melt percolates through the mantle (Burley & Katz,
 92 2015). To constrain the permeability of melt transport, we examined the effects of vary-
 93 ing the permeability coefficient on the seismic properties of the mantle produced by our
 94 1-D model. The thermal structure and porosity was converted to S-wave velocities, as-
 95 suming that melt reduces the velocity by 7.9 % per percent porosity (Hammond & Humphreys,
 96 2000) and including the effects of attenuation (Goes, Armitage, Harmon, Huismans, &
 97 Smith, 2012). Recent joint inversion of teleseismic and ambient noise Rayleigh waves in
 98 Iceland would suggest that the S-wave velocity is between 4 and 3.8 km s⁻¹ at depths
 99 of 50 to 150 km (Harmon & Rychert, 2016) (Figure 1). We find that the permeability
 100 coefficient, k_0 , needs to be relatively high (10^{-5} m²) giving a permeability, $k_\phi = k_0 \phi^3$
 101 (where ϕ is porosity), of the order of 10^{-14} m² ($\phi \approx 0.001$; Figure 1), because other-
 102 wise porosity would be too large and the S-wave velocity would decrease below the ob-
 103 served values. This permeability is an order of magnitude higher than the upper range
 104 used to explore how sea-level change might influence mid-ocean ridge (MOR) magma-
 105 tism (Burley & Katz, 2015; Crowley et al., 2015), and suggests rates of magmatic ascent
 106 of the order of 10 m yr⁻¹, in agreement with MacLennan et al. (2002). Previously it has
 107 been suggested that delays in signal propagation from the zone of partial melting at MORs
 108 to the surface might be of the order of a Milankovitch-scale period, 40 kyr (Huybers &
 109 Langmuir, 2017). However, the high permeability required to match the seismic obser-
 110 vations from Iceland implies a magmatic system that much more rapidly responds to change
 111 in melting conditions, consistent with the fast transport rates estimated from U-series
 112 isotope studies (Elliot & Spiegelman, 2014).

113 **2.2 Glacial Forcing Throughout the Pleistocene**

114 Iceland experienced extensive ice-cover during the last glacial period (Patton, Hub-
 115 bard, Bradwell, & Schomackere, 2017), with maximum thicknesses in the center of the
 116 island of ~ 2km attained by ~23 ka (Figure 2a and b). Deglaciation after the LGM oc-
 117 curred at a varying rate, and was discontinuous. For example, a stage of re-advance oc-

curred during the colder climate of the Younger Dryas (11.7-12.9 ka) (Nordahl & Ingólfsson, 2015). The final phase of deglaciation was particularly rapid, with the main volcanic zones being largely ice free by \sim 10 ka (Figure 2a). The most uncertain period of the glacial history is the pre-LGM growth of the ice sheet. To create the ice sheet histories shown in Figure 2b and Figure 3a we calibrated the ice volume since the LGM against the North Greenland Ice Core Project (NGRIP) $\delta^{18}\text{O}$ record, and Quaternary sea-level curves assuming a linear correlation between these three signals (see Supplementary Material Text S1). We focus on two scenarios: M1, based on the ICE-5G sea-level curves (Peltier, 2004), and M2, based on the sea-level curves of Pico, Creveling, and Mitrovica (2017) (Figure S2).

3 Results

3.1 Effect of glacial loading and unloading

We force our melt model with the 120 ka glacial history after a 5 Myr model wind-up to steady state (model M1, Figure 2b) and using a single value for the ice thickness at each time-step, therefore neglecting the effects of the distal parts of the ice sheet on melting beneath the rift margins. The model predicts peaks in magmatic output and CO_2 flux as pressure changes due to loading and unloading impact the melt production rate (Figure 2). The response of the magmatic system to changes in ice cover varies depending on the mantle upwelling rate, the rate-of-change in ice sheet thickness, and the prior ice sheet history. Glacial loading suppresses melt production (Jull & McKenzie, 1996), leading to a decline in magma supply (see Supplementary Material, Figure S3). For example during the period between 35 and 15 ka, the growth of the ice sheet reduces eruption rates below 5 km of melt per Myr (Figure 2c). The recovery from this loading occurs initially in the deepest part of the system as this region is perturbed the least. Recovery is also faster if the mantle upwelling rate is higher, where an upwelling rate of 20 mm yr^{-1} is more responsive than the equivalent 10 mm yr^{-1} model (Figure 2b). Higher rates of change in surface loading will impact melt production more strongly such that small magnitude but rapid deglaciation events, for example at \sim 85 ka, have a relatively large effect on eruption rates (Figure 2c).

The impact of deglaciation events is modulated by the upwelling rate of the solid mantle because the upwelling rate controls the background productivity of the melting model. At slower upwelling rates, i.e. 10 mm yr^{-1} , some periods of deglaciation are not recorded in the flux of magma erupted. An example of this is the warming event at 60 ka (Figure 2), where the 10 mm yr^{-1} upwelling model produces no response in either the eruption rate or CO_2 flux. If however upwelling is more rapid, 20 mm yr^{-1} , then there is a clear pulse in melt eruption rate (Figure 2). For a more productive scenario, there is increased shallow melting. The displacement imposed by the flexural response to unloading dissipates with depth. Therefore, if melting is productive and hence shallow it will feel the effects of the unloading to a greater extent when compared to a less productive melting system. Furthermore, when productivity is low, the porosity is low and the rate of vertical melt flow is slow such that a pulse in melt production will not reach the surface rapidly.

The magnitude of CO_2 flux peaks are not linearly related to the magnitude in eruption rates (Figure 2d). For example, in the 20 mm yr^{-1} upwelling rate model, the largest CO_2 peak is estimated to occur at \sim 60 ka and not during the volumetrically larger magmatic pulse at the end of the Pleistocene (Figure 2d). This difference is because when the \sim 60 ka warming occurred, the melt was enriched in carbon due to the preceding rapid glaciation. Magma supplied from the mantle during the Late-Pleistocene pulse were more depleted in carbon compared to those in the 60 ka event. The implication of this result is that volumetrically small volcanic events might have just as a strong influence on CO_2

168 degassing as the more significant periods of volcanic eruptions, and the magnitude of CO₂
 169 degassing is dependent on the history of glacial forcing.

170 3.2 Glacial Forcing Through the Latest Pleistocene and Holocene

171 During the last 40 ka, our model suggest that CO₂ flux is highly dependent on the
 172 glacial forcing. There are two distinct late Pleistocene magmatic pulses, separated by
 173 the Younger Dryas cold period (Figure 3a and b). However, for the model M2 ice sheet
 174 history there are three pulses in CO₂ flux at the end of the Pleistocene, due to the faster
 175 ice sheet growth entering the LGM from 35 to 25 ka in this model (Figure 3a and e). This
 176 peak in CO₂ flux is because the small magnitude but rapid deglaciations after 25 ka tap
 177 melts rich in trace elements including Nb and carbon (Figure 3c and d).

178 The observed time series of incompatible trace element concentrations in Icelandic
 179 magmas and ice sheet history have been suggested to be strongly associated (Eason et
 180 al., 2015; Gee et al., 1998; Jull & McKenzie, 1996; MacLennan et al., 2002; Sinton et al.,
 181 2005). Of these studies Gee et al. (1998) and Eason et al. (2015) report on the Nb com-
 182 position of lavas erupted and give age ranges for the erupted lavas. Dating lava flow in
 183 Iceland is complex given the lack of reliable markers from which ages can be obtained.
 184 This means that ages are instead typically taken from the morphology and tephrochronol-
 185 ogy of erupted flows (MacLennan et al., 2002), which is subjective and open to debate.
 186 We therefore must take the age ranges for the Nb compositions reported by Gee et al.
 187 (1998) and Eason et al. (2015) as indicative. We therefore chose to bin the ages into 2.5 kyr
 188 intervals from 0 to 17.5 ka and then at 5 kyr intervals (Figure 3c). The reduction in Nb
 189 compositions plotted is in line with the trends observed within the more selective La and
 190 Sm data set presented in MacLennan et al. (2002), and is therefore likely robust.

191 We find that the predicted change in Nb from all our models fits within the range
 192 of the observations (Figure 3c). The M2 model gives the strongest signature in Nb con-
 193 centrations of deglaciation during the end of the Pleistocene, while the signature is more
 194 subdued in the M1 ice sheet model (Figure 3c). The 1D forward model used is highly
 195 idealised, and yet the agreement between the observations and model is encouraging, and
 196 suggests the compositional change observed in lavas erupted during the late-Pleistocene
 197 to early Holocene is due to rapid deglaciation (Eason et al., 2015; Gee et al., 1998; Maclen-
 198 nan et al., 2002; Sinton et al., 2005). This implies that the observed change in melt com-
 199 position is due to change in ice sheet loading and that the pre-deglaciation volcanism
 200 likely released a significant volume of CO₂ (Figure 3e).

201 The 1D column model will underestimate the impact of change in deep melt pro-
 202 ductivity, as it cannot capture the deep wings of the zone of partial melting. To explore
 203 the impact of this we force a series of 1D models with the vertical flow taken from steady
 204 state corner flow perturbed by the flexural response of the deglaciation of a 200 km wide
 205 ice sheet. The half spreading rate is assumed to be 10 mm yr⁻¹, and the mantle poten-
 206 tial temperature is 1450 °C. Melt travels vertically from the zone of partial melting in
 207 columns at 0 to 80 km from the rift axis (Figure 4). The steady state thickness of melt
 208 erupted at the surface of the simplified 2D model is 15 km (Figure S4), and glacial forc-
 209 ing causes this thickness to vary around this value by the order of 10 km except for a large
 210 spike at the LGM. The crust of Iceland varies in thickness from 20 to 40 km (e.g. Jenk-
 211 ins et al., 2018), and therefore a model steady state thickness of 15 km is a reasonable
 212 lower end-member prediction given that the crust is made of both extrusions and intru-
 213 sions.

214 After glacial perturbation we find that in the central zone, from the ridge centre
 215 to 40 km distance, the trend in Nb and CO₂ flux is relatively similar, with a reduction
 216 in Nb at 15 ka. At distances greater than 40 km, a peak in Nb and CO₂ flux is predicted
 217 to occur with an increasing delay compared to the centre of extension (Figure 4). This
 218 delay is due to the greater distance that the melt has to travel along the vertical path

from the top of the melt zone to the surface at increasing distance from the centre of extension. In full 2D models the distal melt will pool as it migrates laterally towards the centre of extension (Katz, 2008), yet the difference in ascent velocity due to the increase porosity as the melt pools would likely not be sufficient to overcome the increased distance that the signal will have to travel.

The full solution to the coupled equations of magma dynamics would suggest that melts generated at a distance of up to 60 km from the centre of extension are advected to the ridge axis (Katz, 2008). If all of the melt generated up to 60 km from the centre of extension is erupted, then the CO₂ flux is significantly increased during the Holocene due to the addition input of melt from the distal parts of the zone of partial melting (Figure 4b). Therefore these low productivity and deep regions of the zone of partial melting might be a key exporter of mantle carbon into the atmosphere. However, the range of observed Nb concentrations are relatively similar to the axial concentrations, from within <40 km of the rift centre (Figure 4). This would suggest that the widest regions of the zone of partial melting are not sampled by the volcanism in the Reykjanes Ridge and Western Volcanic Zone, leading to an estimate of CO₂ fluxes more in line with the simpler 1D model.

4 Discussion and Conclusions

The models imply that the deglaciation beginning at 18 ka and continuing through the Bolling warming at 14.8 ka released substantial quantities of CO₂ when compared to the last 120 ka (Figure 3c and Figure 4b), and this elevated CO₂ release was because of the preceding growth of the ice sheet. Volcanism during this time would have taken place in a sub-glacial environment and unsurprisingly does not feature in the post-glacial sub-aerial record. Evidence from sub-glacial volcanic units (tuyas) erupted during this time period (Hartley, Thordarson, & de Joux, 2016) suggest volumetric and compositional trends consistent with those predicted by our model (Figure 3c and Figure 4).

Forcing our model with the long-term 120 ka ice sheet history produces a periodic fluxing of CO₂ from Icelandic volcanoes due to ice-loss events over this period, implying a close link between ice dynamics and magmatic out-gassing. The greatest release of CO₂, however, occurred during the period of ice-loss just before the Younger Dryas (~14 ka), and therefore before the largest phase of late-Pleistocene deglaciation (Figure 4). The concentration of CO₂ released in this magmatic pulse was enhanced due to the lack of any significant loss of ice volume since ~40 ka. This created a magmatic system capable of fluxing large volumes of carbon during the initial period of post-LGM deglaciation (both models M1 and M2, Figure 3e), possibly contributing to the increased atmospheric CO₂ levels thought to be recorded between 15 and 14 ka in the EPICA Dome C ice core (Köhler, Knorr, Buiiron, Lourantou, & Chappellaz, 2011). It is therefore possible that this pulse of magmagenic CO₂, from Iceland and elsewhere (e.g. /citephuybers-2009, bolstered the climate warming, and final phase of deglaciation, that proceeded the Younger Dryas.

The CO₂ flux due to deglaciation is strongly influenced by the ice sheet history. Mantle CO₂ flux does not follow a linear relationship with eruption rates: large peaks in CO₂ are also predicted for periods in time when the volume flux is not very high (Figure 2d and 3e). In effect we cannot conclude that all deglaciation events, or other rapid unloading events due to for example erosion (e.g. Sternai, Caricchi, Castelltort, & Chambagnac, 2016), lead to a large flux of volatile gases into the Earths atmosphere. The Earth system is more complex than such simple causality, yet one clear implication is that deglaciation after a prolonged period of ice-house conditions will lead to a significant carbon degassing of the upper mantle.

268 **Supporting Information**

269 A detailed discussion of the methodology can be found in the supporting informa-
 270 tion (Andersen et al., 2004; Andrews, 2008; Armitage, Collier, Minshull, & Henstock, 2011;
 271 Clark et al., 2009; Geirsdóttir, 2011; Gibson & Geist, 2010; Gurenko & Chaussidon, 1995;
 272 Katz, Spiegelman, & Langmuir, 2003; Lambeck & Chappel, 2001; Lambeck, Rouby, Pur-
 273 cell, Sun, & Sambridge, 2014; McKenzie & O’Nions, 1991; Miller, Zhu, Montési, & Gae-
 274 tani, 2014; Ribe, 1985; Scott, 1992; Shorttle & MacLennan, 2011; Silbeck, 1975; Sleep &
 275 Snell, 1976; Spiegelman, 1996; Spratt & Lisicki, 2016).

276 **Acknowledgments**

277 We would like to thank M. A. Mary Gee (The University of Western Australia) for shar-
 278 ing her Nb composition data from the Reykjanes Peninsula, and Tamara Pico (Harvard
 279 University) for sharing her sea level curves. John J. Armitage acknowledges funding from
 280 an Agence National de la Recherche (France), Accueil de Chercheurs de Haute Niveau,
 281 grant InterRift. The 1-D melting model is available from <https://bitbucket.com/johnjarmitage/melt1d-icesheet/>

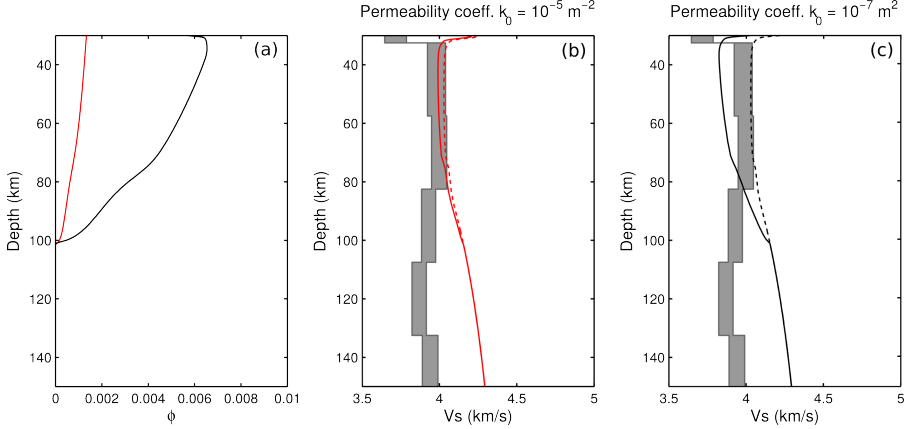
283 **References**

- 284 Andersen, K. K., Azuma, N., Barnola, J. M., Bigler, M., Biscaye, P., Caillon, N.,
 285 ... White, J. W. C. (2004). High-resolution record of northern hemisphere
 286 climate extending into the last interglacial period. *Nature*, *431*, 174-151. (doi:
 287 10.1038/nature02805)
- 288 Andrews, J. T. (2008). The role of the Iceland Ice Sheet in the North Atlantic dur-
 289 ing the late Quaternary: a review and evidence from Denmark Strait. *Journal*
 290 *of Quaternary Science*, *23*, 3-20. (doi: 10.1002/jqs.1142)
- 291 Armitage, J. J., Collier, J. S., Minshull, T. A., & Henstock, T. J. (2011). Thin
 292 oceanic crust and flood basalts: India-Seychelles breakup. *Geochemistry Geo-*
 293 *physics Geosystems*, *12*(Q0AB07). (doi:10.1029/2010GC003316)
- 294 Burley, J. M. A., & Katz, R. F. (2015). Variations in mid-ocean ridge CO₂ emis-
 295 sions driven by glacial cycles. *Earth and Planetary Science Letters*, *426*, 246-
 296 258. (doi: 10.1016/j.epsl.2015.06.031)
- 297 Clark, P. U., Dyle, A. S., Shakun, J. D., Carlson, A. E., Clark, J., Wohlfarth, B., ...
 298 McCabe, A. M. (2009). The last glacial maximum. *Science*, *325*, 710. (doi:
 299 10.1126/science.1172873)
- 300 Crowley, J. W., Katz, R. F., Huybers, P., Langmuir, C. H., & Park, S. H. (2015).
 301 Glacial cycles drive variations in the production of oceanic crust. *Science*, *347*,
 302 1237-1240. (doi: 10.1126/science.1261508)
- 303 Dasgupta, R., & Hirschmann, M. M. (2010). The deep carbon cycle and melting
 304 in Earth’s interior. *Earth and Planetary Science Letters*, *298*, 1-13. (doi:
 305 10.1016/j.epsl.2010.06.039)
- 306 Eason, D. E., Sinton, J. M., Gronvöld, K., & Kurz, M. D. (2015). Effects of
 307 deglaciation on the petrology and eruptive history of the Western Volcanic
 308 Zone, Iceland. *Bulletin of Volcanology*, *77*(47). (doi: 10.1007/s00445-015-0916-
 309 0)
- 310 Elliot, T., & Spiegelman, M. (2014). Melt migration in oceanic crustal production:
 311 A u-series perspective. In *Treatise on geochemistry* (2nd ed., p. 543-581). Else-
 312 vier. (doi: 10.1016/B978-0-08-095975-7.00317-X)
- 313 Gee, M. A. M., Taylor, R. N., Thirwall, M., & Murton, B. J. (1998). Glacioisostacy
 314 controls chemical and isotopic characteristics of tholeiites from the Reykjanes
 315 Peninsula, SW Iceland. *Earth and Planetary Science Letters*, *164*, 1-5.
- 316 Geirsdóttir, A. (2011). Pliocene and pleistocene glaciations of iceland: a brief
 317 overview of the glacial history. In J. Ehlers, P. L. Gibbard, & P. Hughes
 318 (Eds.), *Quaternary glaciations - extent and chronology, a closer look* (Vol. 15,

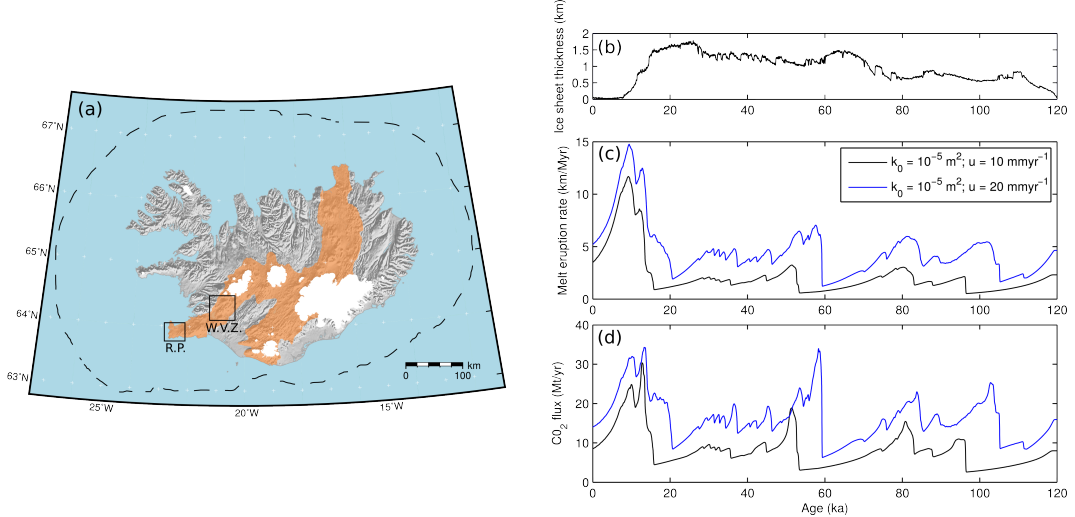
- 319 p. 199-210). Elsevier. (doi: 10.1016/B978-0-444-53447-7.00016-7)
- 320 Gibson, S. A., & Geist, D. (2010). Geochemical and geophysical estimates of litho-
321 spheric thickness variation beneath galápagos. *Earth and Planetary Science
Letters*, *300*, 275-286. (doi: 10.1016/j.epsl.2010.10.002)
- 322 Glazner, A. F., Manley, C. R., Marron, J. S., & Rojstaczer, S. (1999). Fire
323 or ice: Anticorrelation of volcanism and glaciation in california over the
324 past 800,000 years. *Geophysical Resaerch Letters*, *26*, 1759-1762. (doi:
325 10.1029/1999GL900333)
- 326 Goes, S., Armitage, J. J., Harmon, N., Huismans, R., & Smith, H. (2012). Low seis-
327 mic velocities below mid-ocean ridges: Attenuation vs. melt retention. *Journal
328 of Geophysical Research*, *117*, B12403. (doi: 10.1029/2012JB009637)
- 329 Gurenko, A. A., & Chaussidon, M. (1995). Enriched and depleted primitive melts
330 included in olivine from icelandic tholeiites: Origin by continuous melting of a
331 single mantle column. *Geochimica et Cosmochimica Acta*, *59*, 2905-2917.
- 332 Hammond, W. C., & Humphreys, E. D. (2000). Upper mantle seismic wave ve-
333 locity: Effects of realistic partial melt geometries. *Journal of Geophysical Re-
334 search*, *105*, 10975-10986.
- 335 Harmon, N., & Rychert, C. A. (2016). Joint inversion of teleseismic and ambient
336 noise Rayleigh waves for phase velocity maps, an application to Iceland. *Jour-
337 nal of Geophysical Research*, *121*, 5966-5987. (doi: 10.1002/2016JB012934)
- 338 Hartley, M. E., Thordarson, T., & de Joux, A. (2016). Postglacial eruptive history
339 of the Askja region, North Iceland. *Bulleting of Volcanology*, *78*(28). (doi:
340 10.1007/s00445-016-1022-7)
- 341 Huybers, P., & Langmuir, C. H. (2009). Feedback between deglacation, volca-
342 nism, and atmospheric CO₂. *Earth and Planetary Science Letters*, *286*, 479-491.
343 (doi: 10.1016/j.epsl.2009.07.014)
- 344 Huybers, P., & Langmuir, C. H. (2017). Delayed CO₂ emissions from mid-ocean
345 ridge volcanism as a possible cause of late-Pleistocene glacial cycles. *Earth and
346 Planetary Science Letters*, *457*, 238-249. (doi: 10.1016/j.epsl.2016.09.021)
- 347 Jellinek, M. A., Mange, M., & Saar, M. O. (2004). Did melting glaciers
348 cause volcanic eruptions in eastern california? probing the mechanisms
349 of dike formation. *Journal of Geophysical Research*, *109*(B09206). (doi:
350 10.1029/2004JB002978)
- 351 Jenkins, J., Maclennan, J., Green, R. G., Cottaar, S., Deuss, A. F., & White, R. S.
352 (2018). Crustal formation on a spreading ridge above a mantle plume: Re-
353 ceiver function imaging of the Icelandic crust. *Journal of Geophysical Re-
354 search*, *123*, 5190-5208. (doi: 10.1029/2017JB015121)
- 355 Jull, M., & McKenzie, D. (1996). The effect of deglaciation on mantle melting be-
356 neath Iceland. *Journal of Geophysical Research*, *101*(B10), 21815-21828.
- 357 Katz, R. F. (2008). Magma dynamics with the enthalpy method: Benchmark so-
358 lutions and magmatic focusing at mid-ocean ridges. *Journal of Petrology*, *49*,
359 2099-2121. (doi:10.1093/petrology/egn058)
- 360 Katz, R. F., Spiegelman, M., & Langmuir, C. H. (2003). A new parameterization of
361 hydrous mantle melting. *Geochemistry Geophysics Geosystems*, *4*, 1073. (doi:
362 10.1029/2002GC000433)
- 363 Köhler, P., Knorr, G., Buiron, D., Lourantou, A., & Chappellaz, J. (2011). Abrupt
364 rise in atmospheric CO₂ at the onset of the Bolling/Allerod: in-situ ice core
365 data versus true atmospheric signals. *Climate of the Past*, *7*, 473-486. (doi:
366 10.5194/cp-7-473-2011)
- 367 Lambeck, K., & Chappel, J. (2001). Sea level change through the last glacial cycles.
368 *Science*, *292*, 679-686. (doi: 10.1126/science.1059549)
- 369 Lambeck, K., Rouby, H., Purcell, A., Sun, Y., & Sambridge, M. (2014). Sea level
370 and global ice volumes from the Last Glacial Maximum to the Holocene.
371 *Proceedings of the National Academy of Sciences*, *111*, 15296-15303. (doi:
372 10.1073/pnas.141176211)
- 373

- 374 Lund, D. C., & Asimow, P. D. (2011). Does sea level influence mid-ocean ridge mag-
 375 matism on Milankovitch timescales? *Geochemistry Geophysics Geosystems*,
 376 12(Q12009). (doi: 10.1029/2011GC003693)
- 377 Maclennan, J., Jull, M., McKenzie, D., Slater, L., & Gronvöld, K. (2002). The
 378 link between volcanism and deglaciation in Iceland. *Geochemistry Geophysics
 379 Geosystems*, 3(11, 1062). (doi: 10.1029/2001GC000282)
- 380 McKenzie, D., & O'Nions, R. K. (1991). Partial melt distribution from inversion of
 381 rare earth element concentrations. *Journal of Petrology*, 32, 1021-1091.
- 382 Miller, K. J., Zhu, W., Montési, L. G. J., & Gaetani, G. A. (2014). Experimental
 383 quantification of permeability of partially molten mantle rock. *Earth and Plan-
 384 etary Science Letters*, 388, 273-282. (doi: 10.1016/j.epsl.2013.12.003)
- 385 Nordahl, H., & Ingólfsson, O. (2015). Collapse of the Icelandic ice sheet controlled
 386 by sea level rise? *Arktos*, 1, 1-13. (doi: 10.1007/s41063-015-0020-x)
- 387 Pagli, C., & Sigmundsson, F. (2008). Will present day glacier retreat increase
 388 volcanic activity? stress induced by recent glacier retreat and its effect on
 389 magmatism at the Vatnajökull ice cap, Iceland. *Geophysical Research Letters*,
 390 35(L09304). (doi: 10.1029/2008GL033510)
- 391 Patton, H., Hubbard, A., Bradwell, T., & Schomackere, A. (2017). The configura-
 392 tion, sensitivity and rapid retreat of the Late Weichselian Icelandic ice sheet.
 393 *Earth-Science Reviews*, 166, 223-245. (doi: 10.1016/j.earscirev.2017.02.001)
- 394 Peltier, W. R. (2004). Global glacial isostacy and the surface of the ice-age Earth:
 395 The ICE-5G (VM2) model and grace. *Annual Reviews of Earth and Planetary
 396 Science*, 32, 111-149. (2004)
- 397 Pico, T., Creveling, J. R., & Mitrovica, J. X. (2017). Sea-level records from the
 398 U.S. mid-Atlantic constrain Laurentide Ice Sheet extent during Marine Isotope
 399 Stage 3. *Nature Communications*, 8(15621). (doi: 10.1038/ncomms15612)
- 400 Rawson, H., Pyle, D. M., Mather, T. A., Smith, V. S., Fontijn, K., Lachowycz,
 401 S. M., & Naranjo, J. A. (2016). The magmatic and eruptive response of arc
 402 volcanoes to deglaciation: Insights from southern Chile. *Geology*, 44, 251-254.
 403 (doi: 10.1130/G37504.1)
- 404 Ribe, N. M. (1985). The generation and composition of partial melts in the earth's
 405 mantle. *Earth and Planetary Science Letters*, 73, 361-376.
- 406 Rosenthal, A., Hauri, E. H., & Hirschmann, M. M. (2015). Experimental determi-
 407 nation of C, F, and H partitioning between mantle minerals and carbonated
 408 basalt, CO₂/Ba and CO₂/Nb systematics of partial melting, and the CO₂
 409 contents of basaltic source regions. *Earth and Planetary Science Letters*, 415,
 410 77-87. (doi: 10.1016/j.epsl.2014.11.044)
- 411 Saal, A. E., Hauri, E. H., Langmuir, C. H., & Perfit, M. R. (2002). Vapour un-
 412 dersaturation in primitive mid-ocean-ridge basalt and the volatile content of
 413 Earths upper mantle. *Nature*, 419, 451-455. (doi: 10.1038/nature01073)
- 414 Schmidt, P., Lund, B., Hieronymus, C., Maclennan, J., Arnadottir, T., & Pagli,
 415 C. (2013). Effects of present-day deglaciation in Iceland on mantle melt
 416 production rates. *Journal of Geophysical Research*, 118, 3366-3379. (doi:
 417 10.1002/jgrb.50273)
- 418 Scott, D. R. (1992). Small-scale convection and mantle melting beneath mid-ocean
 419 ridges. In J. Phipps Morgan, D. K. Blackman, & J. M. Sinton (Eds.), *Mantle
 420 flow and melt generation at mid-ocean ridges* (Vol. Geophysical Monograph 71,
 421 p. 327-352). American Geophysical Union.
- 422 Shorttle, O., & Maclennan, J. (2011). Compositional trends of icelandic
 423 basalts: Implications for short-length scale lithological heterogeneity in
 424 mantle plumes. *Geochemistry Geophysics Geosystems*, 12, Q11008. (doi:
 425 10.1029/2011GC003748)
- 426 Sigvaldson, G. E., Annertz, K., & Nilsson, M. (1992). Effect of glacier load-
 427 ing/delowering on volcanism: postglacial volcanic production rate of the Dyn-
 428 gjufjöll area, central Iceland. *Bulletin of Volcanology*, 54, 385-392. (doi:

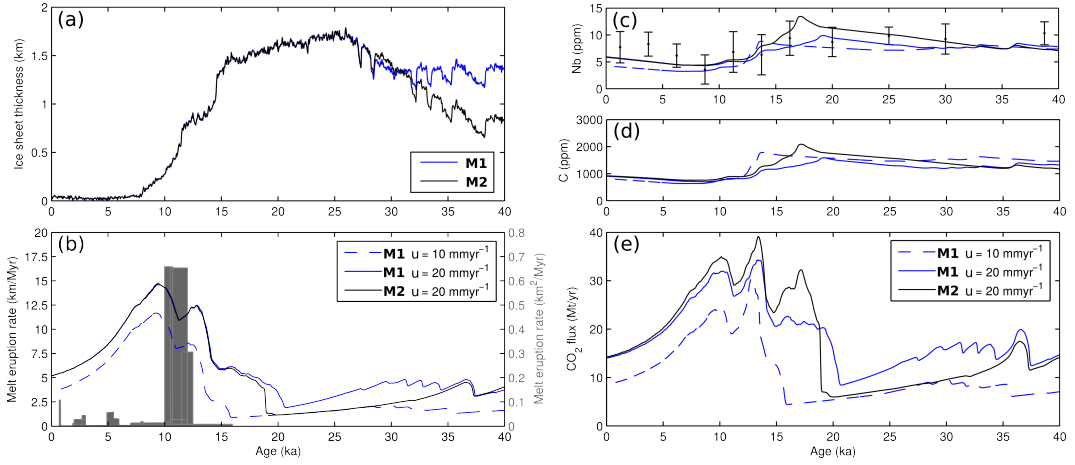
- 429 10.1007/BF00312320)
- 430 Silbeck, J. N. (1975). On the fluid dynamics of ridge crests. In *Notes on the 1975*
431 *summer study program in geophysical fluid dynamics at the Woods Hole Oceanographic*
432 *Institution*, (Vol. 2, p. 113-122).
- 433 Sinton, J., Grönvold, K., & Saemundsson, K. (2005). Postglacial eruptive history
434 of the Western Volcanic Zone, Iceland. *Geochemistry Geophysics Geosystems*,
435 6(Q12006). (doi: 10.1029/2005GC001021)
- 436 Sleep, N. H., & Snell, N. S. (1976). Thermal contraction and flexure of mid-
437 continent and Atlantic marginal basins. *Geophysical Journal of the Royal*
438 *Astronomical Society*, 45, 125-154.
- 439 Spiegelman, M. (1996). Geochemical consequences of melt transport in 2-D: The
440 sensitivity of trace elements to mantle dynamics. *Earth and Planetary Science*
441 *Letters*, 139, 115-132.
- 442 Spratt, R. M., & Lisiecki, L. E. (2016). A late Pleistocene sea level stack. *Climate of*
443 *the Past*, 12, 1079-1092. (doi: 10.5194/cp-12-1079-2016)
- 444 Sternai, P., Caricchi, L., Castelltort, S., & Champagnac, J. D. (2016). Deglaciation
445 and glacial erosion: A joint control on magma productivity by continental unloading.
446 *Geophysical Research Letters*, 43, 1632-1641. (doi:
447 10.1002/2015GL067285)
- 448 Wasylenski, L. E., Baker, M. B., Kent, A. J. R., & Stopler, E. M. (2003). Near-
449 solidus melting of the shallow upper mantle: partial melting experiments on
450 depleted peridotite. *Journal of Petrology*, 44, 116-1191.



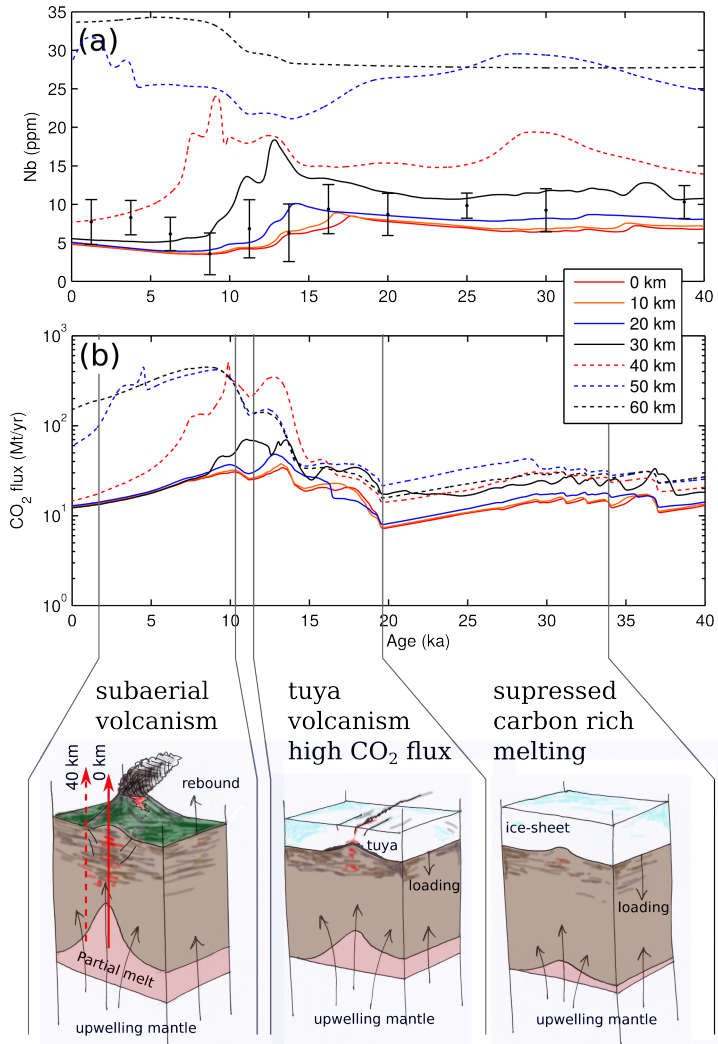
451 **Figure 1.** Profiles of porosity and S-wave seismic velocity for the two model permeabilities of
 452 $k_0 = 10^{-7} \text{ m}^2$ black line, and $k_0 = 10^{-5} \text{ m}^2$ red line. (a) Porosity plotted against depth at steady
 453 state. (b) S-wave velocity from the joint inversion of teleseismic and ambient noise Rayleigh
 454 waves (Harmon & Rychert, 2016) and the predicted S-wave profile from the high permeability
 455 case. The model includes the addition of the adiabatic gradient, the anharmonic effects from the
 456 mineralogy and effects of attenuation (Goes et al., 2012). The dashed line assumes melt has no
 457 effect, the solid line includes a 7.9 % reduction in V_S per percent melt (Hammond & Humphreys,
 458 2000). (c) S-wave velocity predictions for the low permeability case.



459 **Figure 2.** Response of the model to periodic and observed ice sheet thickness changes of the
 460 last 120 ka. (a) Map of Iceland showing the locations of the volcanic rift zones in orange and the
 461 maximum extent of the ice sheet at the last glacial maximum (dashed line). The boxes show the
 462 location of the Reykjanes Peninsular (R. P.) and the Western Volcanic Zone (W. V. Z.). (b) The
 463 ice sheet thickness predicted from the ice sheet model M1 over the last 120 ka. (c) Melt eruption
 464 rate and (d) carbon flux response to the step change in ice sheet thickness: black line, an upper
 465 mantle permeability coefficient of $k_0 = 10^{-5} \text{ m}^2$ and upwelling velocity of 10 mm yr^{-1} , and blue
 466 line, an upwelling velocity of 20 mm yr^{-1} .



467 **Figure 3.** Impact of ice sheet growth and decay on melt eruption and composition over the
468 last 40 ka. (a) Ice sheet models M1 and M2 taken from the sea-level models of Peltier (2004) and
469 Pico et al. (2017) respectively. (b) Melt eruption rates (in km of melt per Myr): blue solid line,
470 ice sheet history 5G for $k_0 = 10^{-5}$ m² with an upwelling rate of 20 mm yr⁻¹; blue dashed line, M1
471 for $k_0 = 10^{-5}$ m² with an upwelling rate of 10 mm yr⁻¹; black solid line, ice sheet history M2 for
472 $k_0 = 10^{-5}$ m² with an upwelling rate of 20 mm yr⁻¹. The gray region shows estimated eruption
473 rates from geological observations [Maclellan et al., 2002] (in km² of melt per Myr). (c) Ob-
474 served and predicted Nb concentrations (ppm), observations are from the Reykjanes Peninsula
475 and the Western Volcanic Zone (Eason et al., 2015; Gee et al., 1998; Sinton et al., 2005) and are
476 binned at 2.5 kyr intervals from 0 to 17.5 ka and then at 5 kyr intervals. (d) Predicted variation of
477 in the concentration of carbon (ppm) within the erupted melt. (e) Predicted variation in the flux
478 of CO₂, assuming that the flux of CO₂ that Icelandic volcanism covers an area of 30,000 km², and
479 CO₂ (ppm) = 3.67 C (ppm) (see Eq. 23 in the Supplementary Material).



480 **Figure 4.** Impact of glacial history on off-axis and on-axis melting. A series of 1D column
 481 melting models forced by the response to deglaciation (ice sheet history model M1) where the
 482 mantle flow is of steady state corner flow. (a) Nb concentrations from the centre of extension out
 483 to 60 km from the centre of extension. The mean concentration weighted by the eruption rate is
 484 plotted as the thick black line. (b) Predicted CO₂ flux from the series of vertical melting models.
 485 The late-Pleistocene eruptions are typified by tuya magmatism. This will have been the case up
 486 until at least ~14 ka, where either magmatism was suppressed or when eruptions occurred they
 487 will have been beneath at least 1 km of ice-cover (Hartley et al., 2016). The suppressed melting
 488 regime will have become carbon rich because the shallow low-C melt production is damped due
 489 to the ice-sheet loading. Upon deglaciation there is increased volcanism, which initially taps the
 490 melt rich carbon.